


Blockchain-assisted virtual power plant framework for providing operating reserve with various distributed energy resources

Hongyi Li, Hongxun Hui and Hongcai Zhang 

ABSTRACT

The paradigm shift from a coal-based power system to a renewable-energy-based power system brings more challenges to the supply-demand balance of the grid. Distributed energy resources (DERs), which can provide operating reserve to the grid, are regarded as a promising solution to compensate for the power fluctuation of the renewable energy resources. Small-scale DERs can be aggregated as a virtual power plant (VPP), which is eligible to bid in the operating reserve market. Since the DERs usually belong to different entities, it is important to investigate the VPP operation framework that coordinates the DERs in a trusted manner. In this paper, we propose a blockchain-assisted operating reserve framework for VPPs that aggregates various DERs. Considering the heterogeneity of various DERs, we propose a unified reserve capacity evaluation method to facilitate the aggregation of DERs. By considering the mismatch between actual available reserve capacity and the estimated value, the performance of VPP in the operating reserve market is improved. A hardware-based experimental system is developed, and numerical results are presented to demonstrate the effectiveness of the proposed framework.

KEYWORDS

Blockchain technology, distributed energy resources, operating reserve, reserve capacity evaluation, virtual power plant.

The decarbonization of the power system leads to an increasing penetration of renewable energy sources (RESs)^[1]. Different from conventional generators, the power outputs of RESs (e.g., photovoltaics and wind turbines) are inherently intermittent and non-dispatchable. The increasing share of RES in generation poses more challenges to the real-time power balancing of the grid, thereby threatens the safety and stability of the power system^[2]. Therefore, the power system requires more operating reserve, to compensate for the fluctuation of the RES generation^[3].

Traditionally, the operating reserve is provided by conventional combustion generators, which are running part-loaded with reduced efficiency. Such efficiency reduction could lead to an increase of fossil fuel usage and thereby bring a devastating effect to the emission reduction brought by RESs^[4]. Thus, researchers propose to use distributed energy resources (DERs), e.g., battery energy storage system (BESS)^[5] and heat, ventilation and air conditioner (HVAC)^[6], to provide operating reserve^[7]. However, the operating reserve provided by a single DER, e.g., an HVAC, is small^[8] and usually cannot meet the minimum entry requirement of the operating reserve markets^[9].

To tackle this problem, one promising solution is to aggregate the DERs as a virtual power plant (VPP)^[10]. Naval et al.^[11] propose a VPP model to aggregate various RES generators and operate them as a single power plant, which reduces grid dependence and electricity costs. Elgamal et al.^[12] propose an optimal scheduling method for RES-based VPP, which reduces the market penalty brought by the intermittency of RES. Xu et al. study a VPP consisting of wind farms and coal-fired plants, which responds to the real-time price signal from the market^[13]. The above-mentioned research only integrates the resources from the generation-side, which might limit the market potential of VPPs^[3].

To actively participate in the electricity markets, researchers study the VPP models that aggregate multiple types of DERs^[14].

Qiu et al.^[15] propose a VPP model with BESS units, generators and interruptible consumers, which bids in both the day-ahead market and the real-time market. Rahimiyan and Baringo^[16] study the optimal coordination of VPP, which consists of generators, flexible loads and storage systems, according to the price signal from the market. Baringo et al.^[17] propose a day-ahead scheduling model for a VPP that aggregates multiple types of DERs and bids in both energy and reserve markets. The above-mentioned studies use a general model for flexible loads in their optimization problem, which neglects the operating characteristics of DERs in the demand-side.

The operating characteristics of DERs in the demand-side are heterogeneous, as they serve different needs^[18]. The unique characteristics of DERs play an important role in the evaluation of the operating reserve capacity that individual DERs can provide. Khani and Farag^[19] develop a BESS model considering the provision of operating reserve. Hui et al.^[20] study the thermal model of the indoor space, atop which they evaluate the reserve capacity that HVACs can provide. The operating reserve capacity evaluation method for inverter-based HVACs, whose power consumption can be continuously adjusted, is proposed in Ref. [21]. Chatterjee et al.^[22] investigate the model of ventilation fans, which provides the correlation between the power consumption and the required airflow. Rotger-Griful et al.^[23] evaluate the potential of ventilation systems for providing operating reserve, considering the dynamics of the indoor carbon dioxide concentration. The above-mentioned studies provide detailed models to describe the electricity consumption behaviors of single-type DERs, while the unified framework that considers the operating reserve capacity evaluation for multiple types of DERs is underdeveloped.

Besides reserve capacity evaluation, another key challenge in VPP operation is the trust crisis^[24]. One typical scenario where the trust crisis could arise from is the process of recording the

response of the DERs for profit allocation^[25]. Since interest conflicts exist between the VPP operator and individual DERs, a centralized ledger maintained by a single entity cannot be fully trusted by the others^[26,27]. In this context, distributed ledger technologies, e.g., blockchain, are preferred due to its widely-recognized credibility, traceability and transparency^[28,29]. Yan et al.^[30] propose a blockchain-based framework for demand response, including the process of invitation, bidding and settlement. Gough et al.^[31] develop a transactive energy model to optimize the power schedule of the DERs within VPP, and record the transaction process with blockchain. Luo et al.^[32] leverage the blockchain smart contract to automatize the power dispatching of multiple DERs. Mnatsakanyan et al.^[33] design a blockchain-mediated VPP model that manages the DERs in a trusted manner. However, there lacks application of blockchain technologies regarding the provision of operating reserve.

As summarized in Table 1, there exist mainly three challenges in aggregating various demand-side DERs in a VPP to provide operating reserve. Firstly, the unique characteristics of individual DERs need to be considered in the evaluation of operating reserve capacity. Secondly, the framework that supports the operating reserve capacity evaluation for multiple types of DERs in the VPP is not well-developed. Finally, the trusted operation of the VPP in providing operating reserve lacks investigation in the existing literature. To fill these research gaps, in this paper, we propose a blockchain-assisted operating reserve framework for VPPs that aggregate DERs of multiple types. The proposed blockchain-assisted framework records the operation process of the VPP in a traceable distributed ledger, which is communally-agreed by all the entities in the VPP, making the operation of VPP trustable. Considering the heterogeneity of DERs, we propose a unified method to evaluate their reserve capacities, such that the DERs can be effectively aggregated to participate in the operating reserve market. With the blockchain smart contract, the operation process of VPP in providing operating reserve is automatized, including the reserve capacity evaluation, the dispensation of regulation signal, the assessment of the response performance and the VPP profit allocation. A compensation mechanism is designed to reduce the response mismatch with the automatic and timely update of operating reserve capacity evaluation, which is enabled by the proposed blockchain framework. Numerical case studies are presented to demonstrate the effectiveness of our proposed method, and the proposed blockchain framework is verified on a hardware-

based experimental system.

The remainder of this paper is organized as follows. Section 1 presents the proposed blockchain-assisted VPP operation framework. Section 2 introduces the unified method for reserve capacity evaluation. In Section 3, a case study is performed to demonstrate the effectiveness of the proposed method. Section 4 concludes the paper.

1 Blockchain-based operation framework of virtual power plant

The blockchain technology can provide immutable, transparent and decentralized recording service to the VPP operation. In this section, the components of the blockchain-based VPP operation framework and their corresponding functionalities are presented.

1.1 Operation framework of virtual power plant

In this paper, we study the VPP that bids in the operating reserve market, where both upward and downward reserve capacities are traded. Providing upward reserve capacity means to decrease the power consumption or feed energy back to the grid. On the contrary, providing downward reserve capacity means to increase the power consumption or feed less energy to the grid. The revenue of providing operating reserve consists of two parts, the capacity revenue and the mileage revenue. The capacity revenue is granted for reserving capacity, which can be calculated before the response. The mileage revenue is calculated based on the actual response to the regulation signal. The operation of VPP consists of four phases, i.e., bidding in the operating reserve market, responding to the regulation signal from the grid, assessing the response performance of the DERs and allocating profit to individual DERs.

1.1.1 Bidding in the operating reserve market

Before the market closure, the VPP collects the reserve capacities estimation P_i^{bid} and capacity price preferences π_i^{cap} from each DER, which will be assembled as the bidding portfolio in the market. The available reserve capacities of heterogeneous DERs are evaluated through a unified method, which will be discussed in detail in the next section.

After the market is cleared, the market equilibrium, i.e., the clearing price, π^{cap} , and the awarded capacity of the VPP, $P_{\text{VPP}}^{\text{cap}}$, are returned to the VPP. According to the market equilibrium, the VPP finds out an index n , which equals to the number of DERs whose bidding is successful, as indicated by the red dotted line in Figure 1.

The awarded capacity of DER i can be expressed as

$$P_i^{\text{cap}} = \begin{cases} P_i^{\text{bid}}, & i < n \\ P_{\text{VPP}}^{\text{cap}} - \sum_{i \in I, i < n} P_i^{\text{cap}}, & i = n \\ 0, & i > n \end{cases}, \forall i \in I, \quad (1)$$

where i is the index of the DERs in price ascending order; I is the set of all DERs in the VPP; P_i^{cap} and P_i^{bid} are the awarded capacity and reserve capacity estimation of DER i , respectively.

1.1.2 Responding to the regulation signal

At the beginning of the operating reserve period, the grid sends a binary direction indicator d and a regulation signal λ to the VPP. The direction indicator $d = 0$ means that the grid needs the VPP to provide upward reserve capacity, while $d = 1$ indicates the needs for downward reserve capacity. As the processes of providing upward and downward reserve capacities are similar, we take providing upward reserve as an example to demonstrate our proposed

Table 1 Summary of related literature

Paper	Various types of DERs	Detailed modeling of demand-side resources	Trusted operation of VPP
[15]	✓	×	×
[16]	✓	×	×
[17]	✓	×	×
[19]	×	✓	×
[20]	×	✓	×
[21]	×	✓	×
[23]	×	✓	×
[30]	×	×	✓
[31]	×	×	✓
[32]	×	×	✓
[33]	×	×	✓
This paper	✓	✓	✓

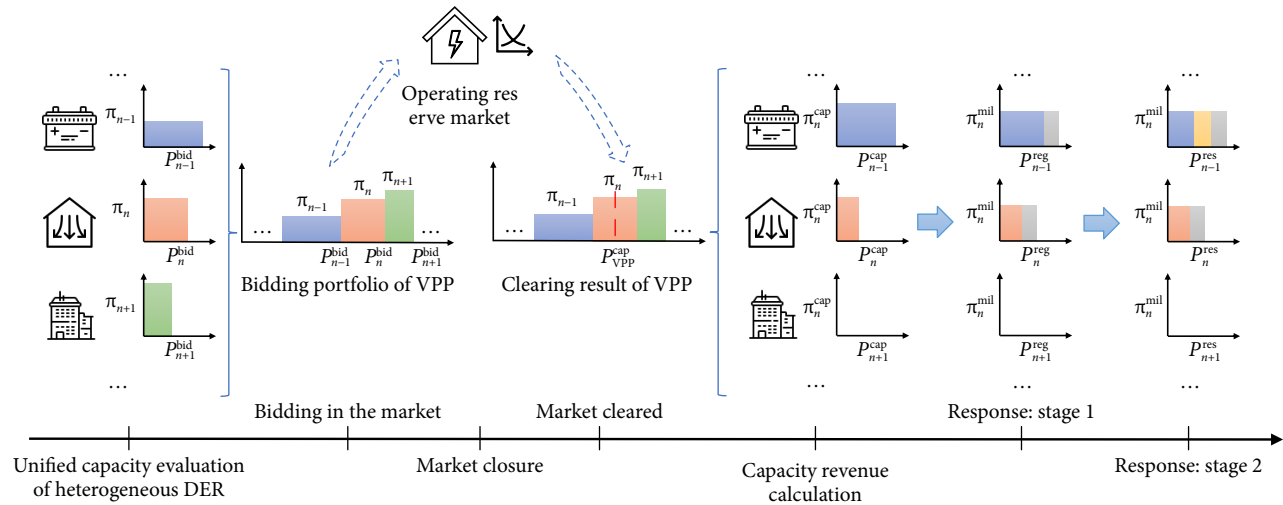


Fig. 1 The process of VPP providing operating reserve for one time slot, including DER reserve capacity evaluation, bidding, regulation signal responding and revenue allocation.

mechanism. Ranging from 0 to 1, the regulation signal λ indicates the amount of reserve capacity needed, which can be calculated as

$$P_{VPP}^{reg} = \lambda P_{VPP}^{cap}, \quad (2)$$

where P_{VPP}^{reg} is the amount of reserve capacity needed of the entire VPP.

Without considering the uncertainty of the DERs, the awarded reserve capacities of DERs are invoked in ascending order of their bidding price preferences. The regulating capacity of each DER, \hat{P}_i^{reg} , can be calculated with Algorithm 1:

Algorithm 1 Calculation of regulating capacity without considering uncertainty of DERs

Initialization: $\hat{P}_i^{reg} = 0, \forall i \in I$

Calculation:

$i \leftarrow 1$

while $i \leq |I|$ **do**

$$\hat{P}_i^{reg} = \min(P_i^{cap}, P_{VPP}^{reg} - \sum_{v \in I} \hat{P}_v^{reg})$$

$i \leftarrow i + 1$

end while

To prevent market participants from speculating by over-estimating their reserve capacity, insufficient response to the regulation signal is penalized by the market. Such penalty motivates the VPP to accurately evaluate its reserve capacity and fully respond to the signal. However, in the VPP, individual DERs might fail to follow the signal accurately due to the uncertainty of its operation. We divide the process of VPP responding to the regulation signal into two stages, namely the calculation of regulating capacity and the response of individual DERs, as shown in Figure 1. The impact of the uncertainty of DERs during these two stages are discussed, as follows.

Stage 1: regulating capacity calculation. Since the reserve capacity of the DER is highly related to its current status, the available capacity of each DER might deviate from its estimated value, leading to a mismatch between the available capacity and the required amount calculated with Algorithm 1. For example, the DER might over-estimate its reserve capacity, as shown by the blue block in Figure 1. The mismatch can be calculated as

$$P_i^{mis,1} = \max(0, \hat{P}_i^{reg} - P_i^t), \quad \forall i \in I, \quad (3)$$

where $P_i^{mis,1}$ is the reserve capacity mismatch of DER i due to uncertainty in Stage 1; P_i^t is the actual available reserve capacity of DER i in real-time.

To avoid sending an infeasible regulation requirement to the DER, the uncertainty of DERs needs to be considered, such that the shortage of reserve capacity of some bid-winning DERs could be compensated before the dispensation of DER regulating capacity. Since the awarded reserve capacity of the VPP is usually not fully invoked, the VPP can assign the regulating capacities of each DER based on their available reserve capacity. For example, in Figure 1, the shortage of reserve capacity is compensated by invoking the available capacity of the next bid-winning DER, which is denoted by the gray block. The regulating capacity that VPP assigns to DER i considering the uncertainty in Stage 1, P_i^{reg} , can be calculated by Algorithm 2:

Algorithm 2 Calculation of regulating capacity considering uncertainty in Stage 1

Initialization: $P_i^{reg} = 0, \forall i \in I$

Calculation:

$i \leftarrow 1$

while $i \leq |I|$ **do**

$$P_i^{reg} = \min(P_i^t, P_{VPP}^{reg} - \sum_{v \in I} P_v^{reg})$$

$i \leftarrow i + 1$

end while

Stage 2: response of individual DERs. Since the DERs are not directly controlled by the VPP, there exists the possibility that the regulation requirements sent by the VPP are not accurately responded, as shown by the yellow box in Figure 1. Different from Stage 1, such insufficient response cannot be compensated, thereby leads to the decrease of the mileage revenue that could be earned.

1.1.3 Assessing the response performance

To help with allocating profit and improving its performance in the market, it is important for the VPP to assess the performance of individual DERs. The mismatch between reserve capacity bids and actual available reserve capacity of each DER is calculated by Algorithm 2. Due to the uncertainty in Stage 2, there might exist a mismatch, $P_i^{mis,2}$, between the assigned regulating capacity, P_i^{reg} , and the actual response of DER i , which can be expressed as

$$P_i^{\text{mis},2} = |P_i^{\text{reg}} - P_i^{\text{res}}|, \forall i \in I, \quad (4)$$

where P_i^{res} denotes the power adjustment of DER i in response to the regulation requirement.

1.1.4 Profit allocation

The profit of each DER for providing operating reserve consists of the capacity revenue, the mileage revenue and the market penalty. In the following paragraphs, we describe the methods to calculate the profit of each DER and the VPP.

Capacity revenue: Based on the market clearing result, the total capacity revenue of the VPP is calculated as

$$R_{\text{VPP}}^{\text{cap}} = \pi^{\text{cap}} P_{\text{VPP}}^{\text{cap}}. \quad (5)$$

On this basis, the capacity revenue of individual DERs can be calculated as

$$R_i^{\text{cap}} = \pi^{\text{cap}} P_i^{\text{cap}}, \forall i \in I. \quad (6)$$

Mileage revenue: The mileage revenue is calculated based on the actual response:

$$R_{\text{VPP}}^{\text{mil}} = \pi^{\text{mil}} \sum_{i \in \mathcal{I}} |P_i^{\text{res}}|, \quad (7)$$

$$R_i^{\text{mil}} = \pi^{\text{mil}} |P_i^{\text{res}}|, \forall i \in I, \quad (8)$$

where π^{mil} denotes the mileage price set by the market.

Market penalty: The inadequate response of the VPP to the regulation signal is penalized by the market, which can be calculated as

$$R_{\text{VPP}}^{\text{pen}} = \pi^{\text{pen}} \left| P_{\text{VPP}}^{\text{reg}} - \sum_{i \in I} P_i^{\text{res}} \right|, \quad (9)$$

where π^{pen} is the penalty rate set by the market.

The VPP penalizes the DERs for the mismatches, and apportions the penalty from the market to related DERs:

$$R_i^{\text{pen}} = \pi^{\text{pen}} (P_i^{\text{mis},1} + P_i^{\text{mis},2}), \forall i \in I. \quad (10)$$

1.2 Blockchain-based realization of the operation framework

1.2.1 Structure and key elements of the blockchain

Since the identity of DERs in the VPP are usually known and vetted, a consortium blockchain framework can be adopted to avoid the costly mining process. In this paper, we realize the proposed VPP operation framework with an open-source consortium blockchain platform, Hyperledger Fabric^[34]. The structure of the blockchain platform is illustrated in Figure 2. The key elements of the blockchain, i.e., peer nodes, distributed ledger and smart contract, are introduced in details in the following paragraphs.

Peer node: Peer nodes are the basic components of the decentralized blockchain network, which act as the container of the distributed ledger and the smart contract. For a consortium blockchain, such as Hyperledger Fabric, the identity of each entity in the VPP is known and vetted. The identity is used by the peer nodes for authentication check before the corresponding entity can interact with the distributed ledger.

Distributed ledger: The distributed ledger consists of a world state database to store the current state of all assets (e.g., timestamp, ID and available reserve capacity) and a temper-resistant blockchain to store the changes of assets (i.e., transactions) in

immutable sequence. Each DER is modeled as a pseudo-asset, of which the properties are represented as a group of key-value pairs. Both the DER itself and the VPP are granted the right to propose changes to the pseudo-assets. Since all changes are recorded in the blockchain and the identities are known, malicious activities can be effectively traced back, thereby enhances the security of the VPP operation.

Smart contract: The smart contract, which is installed on the peer nodes, defines the attributes of the pseudo-asset and the functions that the peer node can utilize to interact with the distributed ledger. To avoid inconsistent changes of the distributed ledger, the smart contract should be agreed by all participants before deployment and remains consistent globally.

1.2.2 Functionalities of blockchain elements

The above-mentioned operation framework defines the principles of interacting with these pseudo-assets. Thus, the VPP operation framework can be integrated to the smart contract and the operation of the VPP can be made reliable, creditable and automatic.

Bidding in the operating reserve market: Before bidding in the operating reserve market for time slot t' , each DER updates its reserve capacity estimation P_i^{bid} and price preference π_i^{cap} . The VPP gathers the information from the DERs by querying the distributed ledger and forms the bidding portfolio. After the operating reserve market is cleared, the market clearing price π^{cap} and the awarded capacity of each DER P_i^{ap} are updated by the VPP.

Responding to the regulation signal: Each DER is assumed to be equipped with a telemetry system, which measures and transfers the indexes related to reserve capacity evaluation, e.g., the indoor temperature of a building cooled by HVAC. Based on such measurements, the reserve capacities of the DERs can be updated periodically, which provide information for the regulating capacity calculation, i.e., Algorithm 2. The regulating capacities P_i^{reg} are updated to the pseudo-asset by the VPP and queried by each DER. The actual response P_i^{res} is measured by the telemetry system, and automatically updated in the distributed ledger.

Assessing the response performance: The reserve capacity mismatches due to the uncertainty in Stage 1 and Stage 2 are calculated according to Eqs. (3) and (4), respectively.

Profit allocation: The capacity revenue and mileage revenue of the bid-winning DERs are calculated through Eqs. (6) and (8). For the mismatches, the penalty of each DER is calculated based on Eq. (10).

2 Unified reserve capacity evaluation of heterogeneous distributed energy resources

VPP can aggregate multiple types of DERs to provide operating reserve. Considering the different physical and operation characteristics, in this section, we introduce a unified evaluation method to assess the available reserve capacities (both upward and downward) of heterogeneous DERs.

In this section, we denote the length of the time slot of providing operating reserve by τ , which starts at time t_1 and ends at time t_2 , i.e., $\tau = t_2 - t_1$. It is assumed that the DER's adjusted power remains constant during each time slot.

2.1 Capacity evaluation of battery energy storage system

When providing upward reserve capacity, BESS discharges to feed energy back to the grid. The maximum discharging power of the BESS at time t , $P_{\text{BESS},t}^{\text{discharge}}$, is constrained by the energy stored in the BESS, E_t , as shown in the following equation:

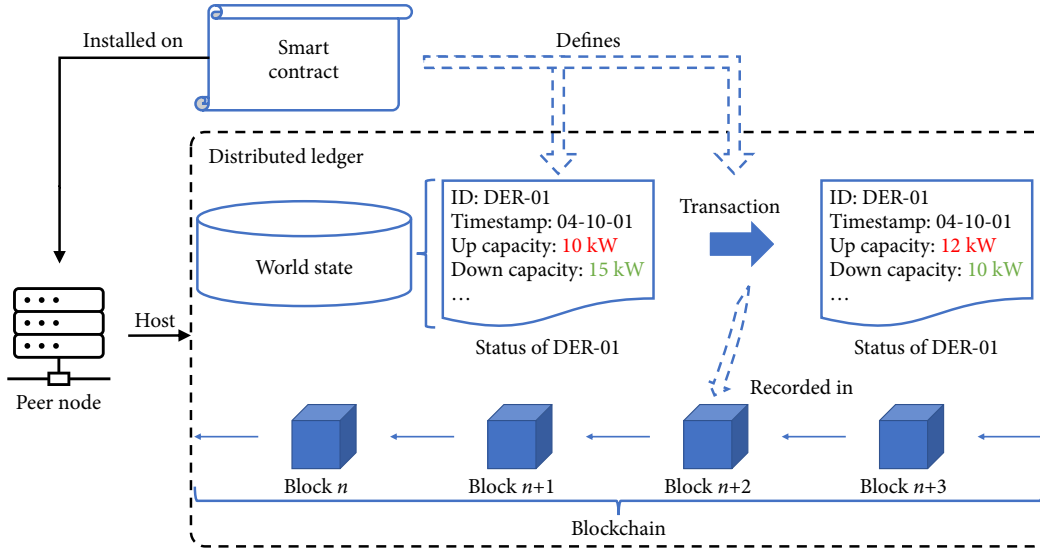


Fig. 2 Structure of the proposed blockchain framework.

$$P_{BESS,t}^{discharge,max} = \min \left\{ P_{BESS}^{min}, \frac{E_{min} - E_t}{\tau} \right\}, \quad (11)$$

where P_{BESS}^{min} is the discharging power limit of the BESS; E_{min} is the lower limit of energy storage of the BESS.

When providing downward reserve capacity, BESS charges to draw energy from the grid. At time t , the maximum charging power of the BESS, $P_{BESS,t}^{charge}$, can be calculated as

$$P_{BESS,t}^{charge,max} = \min \left\{ P_{BESS}^{max}, \frac{E_{max} - E_t}{\tau} \right\}, \quad (12)$$

where P_{BESS}^{max} is the charging power limit of the BESS; E_{max} is the upper limit of the energy storage of the BESS.

The evolution of the energy stored in the BESS can be expressed as

$$E_{t_2} = E_{t_1} + s_{t_1} P_{BESS,t_1}^{charge} \tau - (1 - s_{t_1}) P_{BESS,t_1}^{discharge} \tau, \quad (13)$$

where s_{t_1} is the status indicator of the BESS. We use $s_{t_1} = 1$ to indicate that the BESS is charging during this time slot. Similarly, $s_{t_1} = 0$ indicates that BESS is discharging during this time slot.

The upward and downward reserve capacity that the BESS can provide can be calculated as

$$P_{BESS}^{up} = P_t - P_{BESS,t}^{discharge,max}, \quad (14)$$

$$P_{BESS}^{down} = P_{BESS,t}^{charge,max} - P_t, \quad (15)$$

where P_t is the power of the BESS at time t , without providing operating reserve.

2.2 Capacity evaluation of inverter-based HVAC

To evaluate the reserve capacity of the inverter-based HVAC, the thermal dynamics of the corresponding building needs to be studied, which can be formulated as^[21]

$$C \frac{d\theta_{in}^t}{dt} = H_{cond} + H_{vent} - H_{HVAC}, \quad (16)$$

where C is the thermal capacity of the building; θ_{in}^t is the indoor temperature at time t ; H_{cond} and H_{vent} represent the heat gain through conduction and ventilation, respectively; H_{HVAC} is the cooling capacity of the inverter-based HVAC.

The heat gains can be expressed as a function of the indoor

temperature θ_i :

$$\begin{cases} H_{cond} = (\theta_{out}^t - \theta_{in}^t) / R \\ H_{vent} = C v^t (\theta_{out}^t - \theta_{in}^t) \end{cases}, \quad (17)$$

where θ_{out}^t is the ambient temperature at time t ; R is the building's thermal resistance and v^t is the building's ventilation rate at time t .

The relationship between the cooling capacity H_{HVAC} and the power consumption of the inverter-based HVAC is

$$H_{HVAC} = \eta P_{HVAC}, \quad (18)$$

where η is the energy efficiency ratio; P_{HVAC} is the power consumption of the inverter-based HVAC.

By allowing the indoor temperature to fluctuate within a given range, the power consumption of the inverter-based HVAC can be flexibly adjusted to provide operating reserve.

Rewrite the first order differential equation (16) by substituting Eqs. (17) and (18):

$$\begin{cases} C \frac{d\theta_{in}^t}{dt} = \rho^t (\theta_{out}^t - \theta_{in}^t) - \eta P_{HVAC} \\ \rho^t = \left(\frac{1}{R} + C v^t \right) \end{cases}, \quad (19)$$

where ρ^t indicates the equivalent heat transfer coefficient of the corresponding building at time t .

Integrating both sides of Eq. (19), from t_1 to t_2 :

$$C (\theta_{in}^{t_2} - \theta_{in}^{t_1}) = \int_{t_1}^{t_2} \rho^t \theta_{out}^t dt - \int_{t_1}^{t_2} \rho^t \theta_{in}^t dt - \eta P_{HVAC} \tau. \quad (20)$$

For simplicity, we use the average values of the ambient temperature and the ventilation rate, i.e., θ_{out}^{avg} and v^{avg} , to replace the time-varying values. It is also assumed that the change of the indoor temperature can be well-approximated by a monotonic linear function:

$$\theta_{in}^t = \theta_{in}^{t_1} + \frac{\theta_{in}^{t_2} - \theta_{in}^{t_1}}{t_2 - t_1} (t - t_1), \quad \forall t \in [t_1, t_2]. \quad (21)$$

Reformulating Eq. (20) yields:

$$P_{HVAC} = \frac{\rho^{avg} \theta_{out}^{avg}}{\eta} - \frac{C (\theta_{in}^{t_2} - \theta_{in}^{t_1})}{\eta \tau} - \frac{\rho^{avg} (\theta_{in}^{t_1} + \theta_{in}^{t_2})}{2\eta}. \quad (22)$$

Since the parameters of the building are regarded to be fixed (i.

e., ρ^{avg} , $\theta_{\text{out}}^{\text{avg}}$, η and C are fixed), for the given time slot, the power consumption of the HVAC is deterministic when the indoor temperature at the end of the time slot, θ_{in}^2 , is known:

$$P_{\text{HVAC}} = f_{\text{HVAC}}(\theta_{\text{in}}^1, \theta_{\text{in}}^2, \tau). \quad (23)$$

Assuming that the HVAC is working at cooling mode and the comfortable temperature range of the user is $[\underline{\theta}_{\text{in}}, \overline{\theta}_{\text{in}}]$, the upward and downward reserve capacity of the HVAC can be expressed as

$$P_{\text{HVAC},t}^{\text{up}} = P_{\text{HVAC},t} - \max[f_{\text{HVAC}}(\theta_{\text{in}}^t, \overline{\theta}_{\text{in}}, \tau), P_{\text{HVAC},t}^{\text{min}}], \quad (24)$$

$$P_{\text{HVAC},t}^{\text{down}} = \min[f_{\text{HVAC}}(\theta_{\text{in}}^t, \underline{\theta}_{\text{in}}, \tau), P_{\text{HVAC},t}^{\text{max}}] - P_{\text{HVAC},t}. \quad (25)$$

2.3 Capacity evaluation of car park ventilation system

In car parks, ventilation fans are installed to exhaust the vehicular pollutants and provide fresh air. The concentration of carbon monoxide (CO) is the main concern of the car park ventilation system, which should be remained lower than a specific level. With the assumptions of constant air density, fixed efficiency and no dampers, the model of ventilation fan follows the affinity law^[23]:

$$\frac{Q_1}{Q_2} = \frac{N_1}{N_2}, \quad \frac{p_{s1}}{p_{s2}} = \left(\frac{N_1}{N_2}\right)^2, \quad \frac{P_1}{P_2} = \left(\frac{N_1}{N_2}\right)^3, \quad (26)$$

where Q is the airflow; N is the rotational speed of the fan; p_s is the static pressure of the indoor space; P is the power consumption of the ventilation fan.

When the ventilation fan is driven by a frequency-variable motor, its power can be continuously adjusted. According to the affinity law, the power consumption of the ventilation fan at time t , i.e., $P_{\text{vent},t}$, is determined by the airflow Q_{vent} it provides:

$$P_{\text{vent}} = \left(\frac{Q_{\text{vent}}}{Q_{\text{vent}}^{\text{rated}}}\right)^3 P_{\text{vent}}^{\text{rated}}, \quad (27)$$

where $Q_{\text{vent}}^{\text{rated}}$ and $P_{\text{vent}}^{\text{rated}}$ are the airflow and the corresponding power consumption at rated mode, respectively.

To evaluate the reserve capacity that the ventilation fan can provide, the CO concentration model is developed:

$$V \frac{d\sigma_{\text{in}}^t}{dt} = (Q_{\text{vent}} - q_L^t)(\sigma_{\text{out}}^t - \sigma_{\text{in}}^t) + G^t, \quad (28)$$

where V is the volume of the indoor space; σ_{in}^t is the indoor concentration of CO at time t ; Q_{vent} is the airflow provided by the ventilation fan; q_L^t is the leakage/infiltration airflow at time t ; σ_{out}^t is the ambient CO concentration at time t ; G^t is the CO flow generated in the indoor space at time t .

Taking the integral of both sides of Eq. (28), from t_1 to t_2 , yields:

$$V(\sigma_{\text{in}}^{t_2} - \sigma_{\text{in}}^{t_1}) = \int_{t_1}^{t_2} (Q_{\text{vent}} - q_L^t)(\sigma_{\text{out}}^t - \sigma_{\text{in}}^t) dt + \int_{t_1}^{t_2} G^t dt. \quad (29)$$

To simplify Eq. (29), we use the average values of the leakage/infiltration airflow, the ambient CO concentration and the indoor CO generation, i.e., q_L^{avg} , $\sigma_{\text{out}}^{\text{avg}}$ and G^{avg} , to replace the time-varying values. It is also assumed that the changing of the indoor CO concentration can be well-approximated by a monotonic linear function:

$$\sigma_{\text{in}}^t = \sigma_{\text{in}}^{t_1} + \frac{\sigma_{\text{in}}^{t_2} - \sigma_{\text{in}}^{t_1}}{\tau}(t - \tau), \quad \forall t \in [t_1, t_2]. \quad (30)$$

With the above assumptions, Eq. (29) can be reformulated as

$$Q_{\text{vent}} = V(\sigma_{\text{in}}^{t_2} - \sigma_{\text{in}}^{t_1}) \left[\sigma_{\text{out}}^{\text{avg}} \tau - \frac{\sigma_{\text{in}}^{t_1} + \sigma_{\text{in}}^{t_2}}{2} \tau \right]^{-1} - G^{\text{avg}} \tau \left[\sigma_{\text{out}}^{\text{avg}} \tau - \frac{\sigma_{\text{in}}^{t_1} + \sigma_{\text{in}}^{t_2}}{2} \tau \right]^{-1} + q_L^{\text{avg}}. \quad (31)$$

Since the parameters of the car park, i.e., V , G^{avg} , $\sigma_{\text{out}}^{\text{avg}}$ and q_L^{avg} are constant, for a given time slot, the airflow to be provided by the ventilation system is deterministic when the CO concentration at the end of the interval, $\sigma_{\text{in}}^{t_2}$, is known. Thus, the power consumption of the ventilation system can be calculated as

$$P_{\text{vent}} = f_{\text{vent}}(\sigma_{\text{in}}^1, \sigma_{\text{in}}^2, \tau). \quad (32)$$

When diluting CO, an upper bound, $\overline{\sigma}_{\text{in}}$, is assigned to prevent any harm to health. The reserve capacity of the car park ventilation system can be calculated as

$$P_{\text{vent},t}^{\text{up}} = P_{\text{vent},t} - \max[f_{\text{vent}}(\sigma_{\text{in}}^t, \overline{\sigma}_{\text{in}}, \tau), P_{\text{vent},t}^{\text{min}}], \quad (33)$$

$$P_{\text{vent},t}^{\text{down}} = P_{\text{vent}}^{\text{rated}} - P_{\text{vent},t}. \quad (34)$$

3 Case study

In this section, we introduce the hardware-based experimental system and the blockchain system we used to verify the proposed VPP operation framework. Numerical results are presented to demonstrate the effectiveness of our proposed method.

3.1 System setup

3.1.1 Hardware system

To verify our proposed VPP operation framework, we develop a hardware-based blockchain platform with seven Rock Pi devices^[35], as shown in Figure 3(a). To support the operation of Hyperledger Fabric, we adopt the Rock Pi X version, which is an X86 single-board computer with a 64-bit Intel Cherry Trail quad-core processor. Each Rock Pi X device is equipped with 4 GB of RAM, and a 32-GB SD card. We install Ubuntu 20.04 on each Rock Pi X device, as its operating system. Based on gRPC framework, a communication network between Rock Pi X devices are developed with Go programming language^[36].

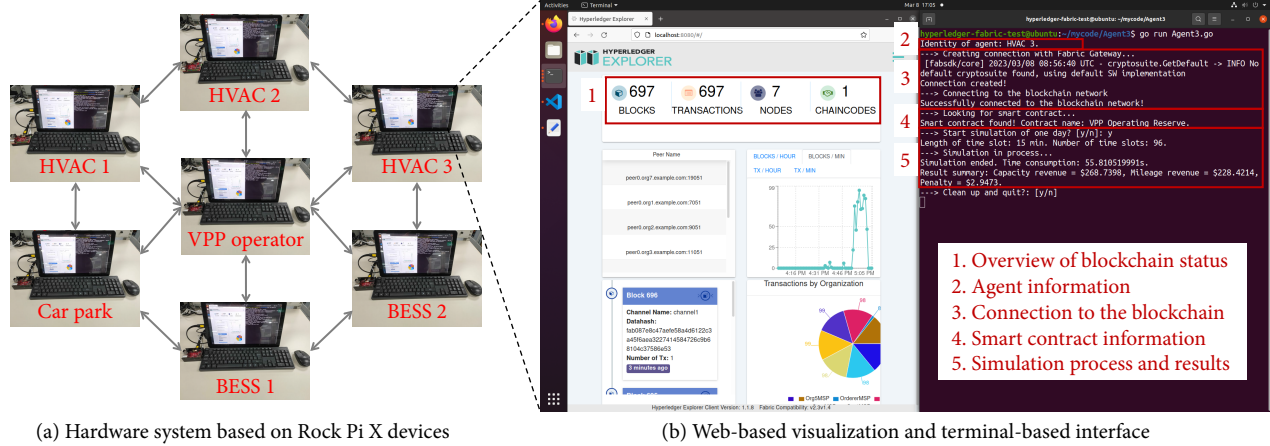
3.1.2 Blockchain system

In this paper, we use Hyperledger Fabric, which is a consortium blockchain platform, to avoid the costly mining process. Specifically, we adopt Hyperledger Fabric v2.3, which has been well verified by developers from different research domains. Hyperledger Fabric also supports the deployment of smart contracts, which allows us to realize our customized functions.

Each Rock Pi X device represents a DER in the VPP, and acts as a peer node in the blockchain system. An X.509 digital certificate is issued to each peer node, which identifies the affiliation of the node. Using the X.509 certificates, the authenticity of each transaction proposal can be verified, which ensures the security of the blockchain. We also configure a web-based front-end page to visualize the activities of the blockchain system, as shown in Figure 3(b).

3.1.3 Virtual power plant

We adopt a VPP with six DERs, including three HVACs, one car park ventilation system and two BESSs, of which the parameters are shown in Table 2. During the operation of VPP, each DER accesses its corresponding peer node to interact with the VPP operator. We develop a terminal-based interface to visualize this process, as shown in Figure 3(b).



(a) Hardware system based on Rock Pi X devices

(b) Web-based visualization and terminal-based interface

Fig. 3 A diagram of the hardware-based experimental system, which is used to verified our proposed blockchain-based VPP operation framework.

3.1.4 Parameters

We simulate the VPP operation for one day, setting the length of each time slot to 15 minutes. The ambient temperature is based on the real historical temperature data of a summer day in Macao. The indoor temperature references of three HVACs are set to 21 °C, 22 °C and 23 °C, respectively. Each HVAC allows an

Table 2 Parameters of individual DERs in VPP

DER	P^{min} (MW)	P^{max} (MW)	Physical constraint
HVAC 1	0	3.6	$20\text{ }^{\circ}\text{C} \leq \theta_{in} \leq 22\text{ }^{\circ}\text{C}$
HVAC 2	0	3.6	$21\text{ }^{\circ}\text{C} \leq \theta_{in} \leq 23\text{ }^{\circ}\text{C}$
HVAC 3	0	3.6	$22\text{ }^{\circ}\text{C} \leq \theta_{in} \leq 24\text{ }^{\circ}\text{C}$
Car park	0	5	$\sigma_{in} \leq 12\text{ ppm}$
BESS 1	-1.5	2	$0 \leq E \leq 2\text{ MW}$
BESS 2	-2	1.8	$0 \leq E \leq 2.2\text{ MW}$

indoor temperature deviation of 1 °C from the reference value, both upward and downward. The ambient CO concentration is set to five parts per million (ppm), while the indoor CO concentration is required to remain below 12 ppm, with a reference value of 10 ppm. Both the two BESSs tend to keep their state of charge levels at 75%.

3.2 Operating reserve market clearing results

For each time slot, the VPP operator collects the bidding information from each DERs, including both upward reserve capacities and downward reserve capacities. Based on the price preferences of the DERs, the VPP operator forms the bidding portfolio and bids in the operating reserve market on behalf of the DERs, as shown in Figures 4 and 5. The bids from individual DERs are sorted in ascending order, as indicated by the stacked blocks. The awarded reserve capacities of the VPP are denoted by the red lines with triangular marks, in both Figures 4 and 5. After the operating reserve market is cleared, the awarded capacity of each DER is

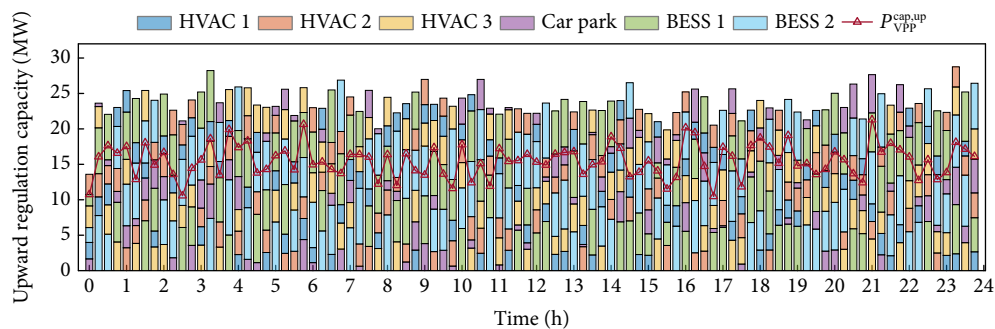


Fig. 4 Upward reserve capacity bidding portfolio and operating reserve market clearing result.

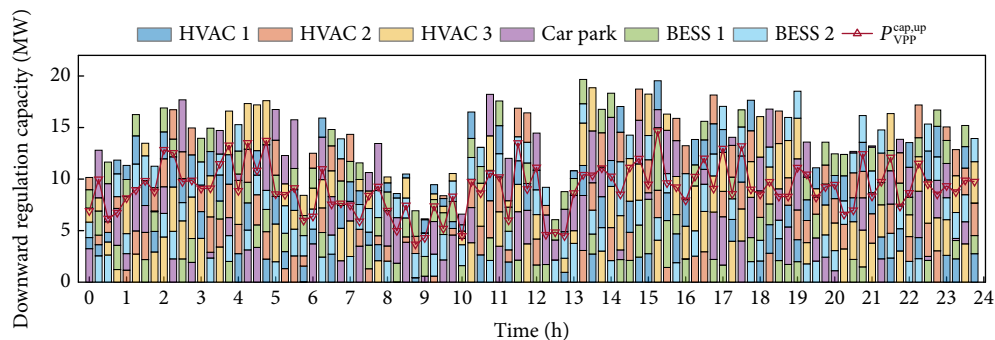


Fig. 5 Downward reserve capacity bidding portfolio and operating reserve market clearing result.

calculated and uploaded to the blockchain by the VPP operator. The capacity revenue can also be calculated, based on the market clearing price, as shown in Table 3.

3.3 Status of distributed energy resources

At the beginning of each time slot, the VPP operator receives the

regulation signal from the grid. Based on Algorithm 2, the VPP operator collects the available capacity of each DER in real-time and calculates the regulating capacity of each DER. The regulating capacity information is uploaded to the blockchain network, and each DER regulates its power outputs accordingly. Regulating the operating power of individual DERs will result in a change of the

Table 3 Revenues and penalties of individual DERs and VPP

Entity	R^{cap} (\$)	R^{mil} (\$)	R^{pen} (\$)		
			w/o	w	Reduction
HVAC 1	187.2849	111.4927	16.3460	4.1143	-74.83%
HVAC 2	205.8219	143.1060	17.7571	4.1825	-76.45%
HVAC 3	268.7398	228.4214	12.3143	2.9473	-76.07%
Car park	189.6944	176.4313	11.1086	5.6599	-49.05%
BESS 1	303.3917	260.0131	21.8779	6.0958	-72.14%
BESS 2	351.6616	188.5902	21.2828	3.9001	-81.68%
VPP	1506.5943	1108.0547	100.6868	26.8998	-73.28%

w and w/o stand for the scenarios with and without blockchain, respectively

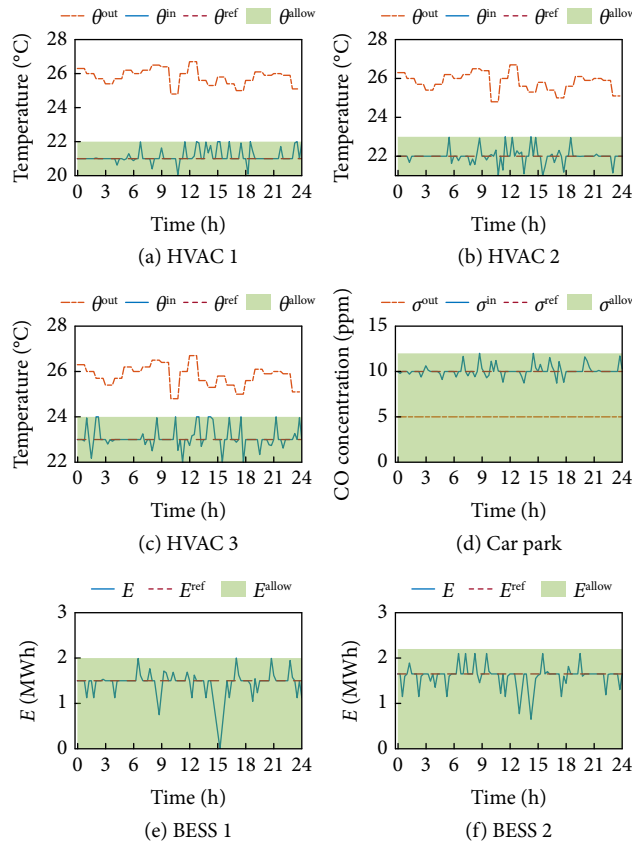


Fig. 6 Daily operation results of different DERs.

statuses of individual DERs, as shown in Figure 6. Although the statuses of DERs, i.e., the indoor temperatures of HVACs, the CO concentration of the car park and the stored energy of the BESSs, vary from their reference values when a regulation signal is received, these statuses always remain in the allowed range, which is indicated by the light green areas. After providing operating reserve, individual DERs regulate their power to restore the statuses to the reference levels, until the next regulation signal is received.

3.4 Reduction in reserve capacity mismatch

As we discussed in the previous sections, there might exist a mismatch between the estimated reserve capacity for bidding and the actual available reserve capacity in real-time. We demonstrate the mismatch and its mitigation with Figure 7. The mismatch resulting from Stage 1 uncertainty takes the majority of the response mismatch, as the area of the green blocks are much larger than the area of the yellow blocks. To mitigate the effect of inaccurate estimation of reserve capacity, we use Algorithm 2 to replace Algorithm 1 in regulating capacity calculation, which is enabled by the proposed blockchain framework. With the blockchain smart contract, the automatic, timely and trusted update of operating reserve capacity evaluation result can be achieved. Thus, the response mismatch resulting from Stage 1 uncertainty, i.e., the green blocks in Figure 7, can be mitigated, as the shortage in reserve capacity is assigned to other DERs. Comparing with the non-blockchain scenario, our proposed framework reduces the reserve capacity mismatch and brings a 73.28% decrease to the penalty of the VPP, as shown in Table 3.

We also demonstrate the compensation for reserve capacity mismatch with the scenario in time slot 45, i.e., from 11:00 a.m. to

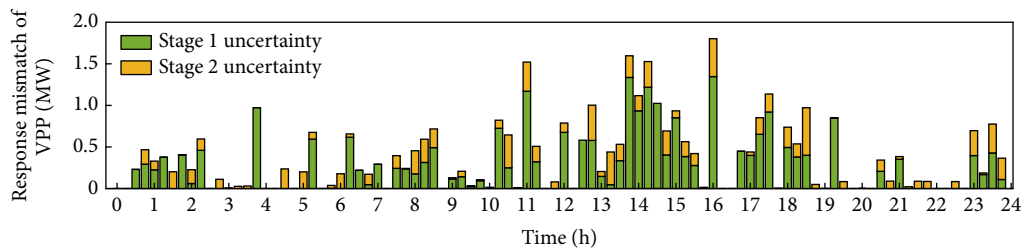


Fig. 7 Mismatch of response to the regulation signal of VPP.

11:15 a.m., as shown in Figure 8. In this time slot, the bid-winning DERs are the car park, HVAC 3 and HVAC 2. When the regulation signal arrives, the actual available capacity of HVAC 3 is less than the estimated value, as denoted by the yellow blocks in Fig. 8. Without the proposed framework, the regulating capacity assigned to HVAC 3 cannot be fully provided, which leads to a penalty from the market. With the proposed blockchain framework, the trusted and timely update of operating reserve capacity evaluation results can be realized. The blockchain smart contract not only automizes the update of capacity evaluation result, but also limits the DER itself to be the only authorized entity to submit an update. In this way, the VPP operator can trust the updated information, be aware of the shortage in the actual available capacity of HVAC 3, and is able to invoke the spare capacity of the car park and HVAC 2 for compensation. By utilizing the spare capacity from other bid-winners, the VPP improves its response performance and reduces the penalty from the market.

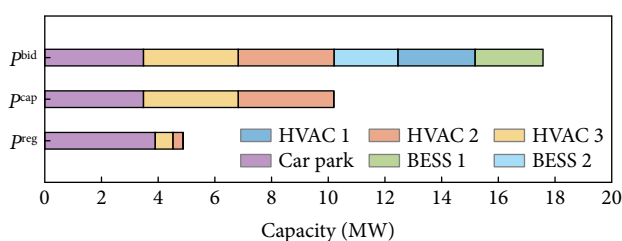


Fig. 8 Compensation for reserve capacity mismatch in time slot 45.

4 Conclusions

In this paper, we propose a blockchain-assisted operating reserve framework for VPPs that aggregates multiple types of DERs. We introduce the process of providing operating reserve to the grid, and define the corresponding functionalities of the blockchain components. Considering the heterogeneity of the DERs, we propose a unified reserve capacity evaluation model to facilitate the aggregation of DERs in the VPP. To mitigate the reserve capacity mismatch due to the uncertainty in DER operation status, we propose a compensation method which considers the available reserve capacity in real-time. The proposed framework is verified with a hardware-based experimental system. The results show that our proposed method can effectively coordinate heterogeneous DERs in the VPP to provide operating reserve, without violating their physical constraints. By evaluating the available reserve capacity in real-time, the market penalty of the VPP can be significantly reduced. In the future works, more aspects, such as the duration of response and the failure of response, can be considered at the stage of DER evaluation to give a more general description of the response capability of DERs, which could further improve the performance of the VPP in providing operating reserve.

Acknowledgements

This paper is funded by The Science and Technology Development Fund, Macau SAR (File No. 0011/2022/AGJ and File No. SKL-IOTSC(UM)-2021-2023).

Article history

Received: 9 March 2023; Revised: 12 June 2023; Accepted: 12 June 2023

Additional information

© 2023 The Author(s). This is an open access article under the CC BY license (<http://creativecommons.org/licenses/by/4.0/>).

Declaration of competing interest

The authors have no competing interests to declare that are relevant to the content of this article.

References

- [1] Strbac, G., Papadaskalopoulos, D., Chrysanthopoulos, N., Estanqueiro, A., Algarvio, H., Lopes, F., de Vries, L., Morales-España, G., Sijm, J., Hernandez-Serna, R., et al. (2021). Decarbonization of electricity systems in Europe: Market design challenges. *IEEE Power and Energy Magazine*, 19: 53–63.
- [2] Guan, Y., Wei, B., Guerrero, J. M., Vasquez, J. C., Gui, Y. (2022). An overview of the operation architectures and energy management system for multiple microgrid clusters. *iEnergy*, 1: 306–314.
- [3] Chen, W., Qiu, J., Zhao, J., Chai, Q., Dong, Z. Y. (2021). Bargaining game-based profit allocation of virtual power plant in frequency regulation market considering battery cycle life. *IEEE Transactions on Smart Grid*, 12: 2913–2928.
- [4] Strbac, G. (2008). Demand side management: Benefits and challenges. *Energy Policy*, 36: 4419–4426.
- [5] Qin, J., Wan, Y., Yu, X., Li, F., Li, C. (2019). Consensus-based distributed coordination between economic dispatch and demand response. *IEEE Transactions on Smart Grid*, 10: 3709–3719.
- [6] Hui, H., Chen, Y., Yang, S., Zhang, H., Jiang, T. (2022). Coordination control of distributed generators and load resources for frequency restoration in isolated urban microgrids. *Applied Energy*, 327: 120116.
- [7] Song, Y., Wan, C., Hu, X., Qin, H., Lao, K. (2022). Resilient power grid for smart city. *iEnergy*, 1: 325–340.
- [8] Yu, P., Zhang, H., Song, Y., Hui, H., Chen, G. (2023). District cooling system control for providing operating reserve based on safe deep reinforcement learning. *IEEE Transactions on Power Systems*.
- [9] Chen, Q., Fang, X., Guo, H., Zheng, K., Tang, Q., Lyu, R., Pan, K., Palensky, P., Kirschen, D. S., Kang, C. (2022). The competition and equilibrium in power markets under decarbonization and decentralization. *iEnergy*, 1: 188–203.
- [10] Bhuiyan, E. A., Hossain, M. Z., Mueen, S. M., Fahim, S. R., Sarker, S. K., Das, S. K. (2021). Towards next generation virtual power plant: Technology review and frameworks. *Renewable and Sustainable Energy Reviews*, 150: 111358.
- [11] Naval, N., Sánchez, R., Yusta, J. M. (2020). A virtual power plant optimal dispatch model with large and small-scale distributed renewable generation. *Renewable Energy*, 151: 57–69.
- [12] Hany Elgamal, A., Kocher-Oberlehner, G., Robu, V., Andoni, M. (2019). Optimization of a multiple-scale renewable energy-based virtual power plant in the UK. *Applied Energy*, 256: 113973.
- [13] Xu, Z. Y., Qu, H. N., Shao, W. H., Xu, W. S. (2016). Virtual power plant-based pricing control for wind/thermal cooperated generation in China. *IEEE Transactions on Systems, Man, and Cybernetics: Systems*, 46: 706–712.
- [14] Wang, Y., Ai, X., Tan, Z., Yan, L., Liu, S. (2016). Interactive dispatch modes and bidding strategy of multiple virtual power plants based on demand response and game theory. *IEEE Transactions on Smart Grid*, 7: 510–519.
- [15] Qiu, J., Meng, K., Zheng, Y., Dong, Z. Y. (2017). Optimal scheduling of distributed energy resources as a virtual power plant in a transactive energy framework. *IET Generation, Transmission & Distribution*, 11: 3417–3427.
- [16] Rahimiyan, M., Baringo, L. (2019). Real-time energy management of a smart virtual power plant. *IET Generation, Transmission & Distribution*, 13: 2015–2023.

- [17] Baringo, A., Baringo, L., Arroyo, J. M. (2019). Day-ahead self-scheduling of a virtual power plant in energy and reserve electricity markets under uncertainty. *IEEE Transactions on Power Systems*, 34: 1881–1894.
- [18] Du, P., Lu, N. (2011). Appliance commitment for household load scheduling. *IEEE Transactions on Smart Grid*, 2: 411–419.
- [19] Khani, H., Farag, H. E. Z. (2019). Joint arbitrage and operating reserve scheduling of energy storage through optimal adaptive allocation of the state of charge. *IEEE Transactions on Sustainable Energy*, 10: 1705–1717.
- [20] Hui, H., Ding, Y., Liu, W., Lin, Y., Song, Y. (2017). Operating reserve evaluation of aggregated air conditioners. *Applied Energy*, 196: 218–228.
- [21] Hui, H., Siano, P., Ding, Y., Yu, P., Song, Y., Zhang, H., Dai, N. (2022). A transactive energy framework for inverter-based HVAC loads in a real-time local electricity market considering distributed energy resources. *IEEE Transactions on Industrial Informatics*, 18: 8409–8421.
- [22] Chatterjee, A., Zhang, L., Xia, X. (2015). Optimization of mine ventilation fan speeds according to ventilation on demand and time of use tariff. *Applied Energy*, 146: 65–73.
- [23] Rotger-Griful, S., Jacobsen, R. H., Nguyen, D., Sørensen, G. (2016). Demand response potential of ventilation systems in residential buildings. *Energy and Buildings*, 121: 1–10.
- [24] Tian, N., Guo, Q., Sun, H., Zhou, X. (2022). Fully privacy-preserving distributed optimization in power systems based on secret sharing. *iEnergy*, 1: 351–362.
- [25] Rahmani-Dabbagh, S., Sheikh-El-Eslami, M. K. (2016). A profit sharing scheme for distributed energy resources integrated into a virtual power plant. *Applied Energy*, 184: 313–328.
- [26] Chen, S., Shen, Z., Zhang, L., Yan, Z., Li, C., Zhang, N., Wu, J. (2021). A trusted energy trading framework by marrying blockchain and optimization. *Advances in Applied Energy*, 2: 100029.
- [27] Chen, S., Zhang, L., Yan, Z., Shen, Z. (2021). A distributed and robust security-constrained economic dispatch algorithm based on blockchain. *IEEE Transactions on Power Systems*, 37: 691–700.
- [28] Zhou, Y., Manea, A. N., Hua, W., Wu, J., Zhou, W., Yu, J., Rahman, S. (2022). Application of distributed ledger technology in distribution networks. *Proceedings of the IEEE*, 110: 1963–1975.
- [29] Chen, S., Mi, H., Ping, J., Yan, Z., Shen, Z., Liu, X., Zhang, N., Xia, Q., Kang, C. (2022). A blockchain consensus mechanism that uses Proof of Solution to optimize energy dispatch and trading. *Nature Energy*, 7: 495–502.
- [30] Yan, Y., Huang, J., Chen, X., Zhang, Z., Zhang, T., Lin, Z. (2022). Blockchain-based framework of power demand response in China. *IET Renewable Power Generation*, 16: 781–791.
- [31] Gough, M., Santos, S. F., Almeida, A., Lotfi, M., Javadi, M. S., Fitiwi, D. Z., Osório, G. J., Castro, R., Catalão, J. P. S. (2022). Blockchain-based transactive energy framework for connected virtual power plants. *IEEE Transactions on Industry Applications*, 58: 986–995.
- [32] Luo, X., Xue, K., Xu, J., Sun, Q., Zhang, Y. (2021). Blockchain based secure data aggregation and distributed power dispatching for microgrids. *IEEE Transactions on Smart Grid*, 12: 5268–5279.
- [33] Mnatsakanyan, A., Albeshr, H., Almarzooqi, A., Iraklis, C., Bilbao, E. (2022). Blockchain mediated virtual power plant: From concept to demonstration. *The Journal of Engineering*, 2022: 732–738.
- [34] Androulaki, E., Barger, A., Bortnikov, V., Cachin, C., Christidis, K., De Caro, A., Enyeart, D., Ferris, C., Laventman, G., Manevich Y. et al. (2018). Hyperledger fabric: A distributed operating system for permissioned blockchains. In: Proceedings of the Thirteenth Eurosys Conference, New York, NY, USA.
- [35] Radxa Limited (2023). ROCK Pi X. Available at <https://wiki.radxa.com/RockpiX>.
- [36] gRPC Authors (2022). Go| gRPC. Available at <https://grpc.io/docs/languages/go/>